Supplementary Information
Vectorial optical field reconstruction by attosecond spectral interferometry.

P. Carpeggiani[1,2†], M. Reduzzi[1,2†], A. Comby[1†], H. Ahmadi[1,3], S. Kühn[4], F. Calegari[2,5,6], M. Nisoli[1,2], F. Frassetto[7], L. Poletto[7], D. Hoff[8], J. Ullrich[9], C. D. Schröter[10], R. Moshammer[10], G. G. Paulus[8], G. Sansone[1,2,4,11].[1]

[1] *(1) Dipartimento di Fisica, Politecnico Piazza Leonardo da Vinci 32, 20133 Milano Italy*
(2) IFN-CNR, Piazza Leonardo da Vinci 32, 20133 Milano Italy
(3) Department of Physical Chemistry,
School of Chemistry, College of Science,
University of Tehran, Tehran, Iran
(4) ELI-ALPS, ELI-Hu Kft., Dugonics ter 13, H-6720 Szeged, Hungary
(5) Deutsches Elektronen-Synchrotron,
Notkestrasse 85, Hamburg 22607, Germany
(6) Physics Department, University of Hamburg,
Luruper Chaussee 149, 22761 Hamburg, Germany
(7) Institute of Photonics and Nanotechnologies,
CNR via Trasea 7, 35131 Padova Italy
(8) Institut für Optik und Quantenelektronik,
Friedrich-Schiller-Universität Jena, Max-Wien-Platz 1, 07743 Jena, Germany
(9) Physikalisch-Technische Bundesanstalt,
Bundesallee 100, 38116 Braunschweig, Germany
(10) Max-Planck-Institut für Kernphysik,
Saupfercheckweg 1, 69117 Heidelberg, Germany
(11) Physikalisches Institut, Albert-Ludwigs-Universität Freiburg, 79106 Freiburg, Germany
† *These authors contributed equally to this work*

(Dated: 12th May 2017)

Experimental setup

Isolated attosecond pulses were generated using CEP-stable few-cycle pulses centered at $\lambda_0 = 744$ nm, with an energy of 600 μJ at 10 kHz repetition rate. Broadband XUV continua were generated in argon by means of the PG technique[1] using a delay plate of birifringent quartz with a thickness of 180 μm and zero-order broadband quarter-wave plate. The intensity of the IR pulse in the temporal window of linear polarisation was estimated in $I \simeq 1.5 \times 10^{14}$ W/cm^2. The XUV radiation was then focused by a toroidal mirror in the interaction region of a Reaction Microscope (REMI) (Fig. 1a)[2], which was used to determine the direction of polarisation of the attosecond pulses generated for $\alpha_1 = 45°$ and $\alpha_2 = -45°$, by measuring the three dimensional photoelectron angular distribution in helium. The measurements are shown in Fig. 1b,c. The main axis of the photoelectron angular distributions, corresponding to the polarisation directions of the XUV radiation in the interaction region of the REMI, were estimated in $\theta_1 = 57° \pm 3°$ and $\theta_2 = 315° \pm 3°$. The error was estimated by fitting the angular projections of the photoelectron distributions with a cosine function.

We characterized the photoelectron angular distributions generated by the attosecond pulses with and without metallic filter (aluminium filter with a thickness of 100 nm). We could not observe any significant difference in the polarisation direction of the XUV radiation in these two conditions. The influence of the two spatially separated XUV sources on the photoelectron measurement was investigated by shifting (without removing) the binary plate to avoid the generation of the two-foci in the focal plane. The polarisation of the XUV pulse measured in this condition coincided with the polarisation of the twin XUV pulses within our experimental uncertainty.

Considering the reflection on the surface of the toroidal mirror (gold at a grazing incidence of 4°) (see Fig. 1a), the polarisation directions of the isolated attosecond pulses in the generation cell are given by: $\gamma_1 = \pi - \theta_1 = 123° \pm 3°$ and $\gamma_2 = \pi - \theta_2 = 225° \pm 3°$. For a multi-order quarter-wave plate, $\Delta\gamma = \gamma_2 - \gamma_1 = 90°$. The deviation of $\Delta\gamma$ from this value was taken into account in the pulse reconstruction.

The different complex reflectivity of the s and p components of the XUV attosecond pulse on the toroidal mirror did not appreciably affect the estimation of the angles $\gamma_{1,2}$. Indeed, the ratio of the amplitudes of the complex reflectivity of the s and p components was

estimated in $r \simeq 1.05$. The deviation from the unitary value corresponds to a rotation of the polarisation axis of the attosecond pulse from the specular direction of only 1.3°. This value is definitely smaller than the error bar (±3°) determined by the uncertainty of the fit of the photoelectron angular distribution. The relative phase shift between the complex reflectivity was estimated in $\Delta\phi_r = 1.5°$. Therefore, the reflection induces a very small degree of ellipticity ($\varepsilon \leq 0.013$) on the incident linearly polarised attosecond pulse that does not affect the reconstruction procedure.

The diverging XUV pulse was analysed by an XUV spectrometer (see Fig. 1a) composed by a cylindrical mirror and a concave grating, which dispersed the spectral components in the focal plane (x-direction), where an MCP coupled to a phosphor screen was placed. In the perpendicular direction (y-direction) the propagation of the two coherent XUV pulses is not affected. A CCD camera acquired the signals at the back of the phosphor screen. A piezoelectric translator was used to change and monitor in step of 20 nm the delay between the driving and unknown fields.

The CEP of the driving pulses were characterized on a single-shot basis using a Stereo-ATI[3]. The measured values were used to pre-compensate the CEP drift using as feedback the acoustic waveforms sent to the Dazzler present in the beam path before the laser amplifier[4]. The maximum intensity of the (linearly polarized) perturbing field used in the experiment was estimated in $I_{unk} = 1.5 \times 10^{11}\mathrm{W/cm^2}$.

Simulations and field reconstruction

The effect of the perturbing (in principle unknown) field on the properties of the high-order harmonic spectra was simulated by solving the Lewenstein integral[5] with the stationary phase method[6], taking into account the total electric field given by the sum of the driving and perturbing fields: $\mathbf{E}_{tot} = \mathbf{E}_{dr} + \mathbf{E}_{unk}$. The total field was used to solve the saddle point equations[7]:

$$\begin{aligned} \omega - \frac{[\mathbf{p}_s - \mathbf{A}_{tot}(t_s)] \cdot [\mathbf{p}_s - \mathbf{A}_{tot}(t_s)]}{2} - I_p = 0 \\ \frac{[\mathbf{p}_s - \mathbf{A}_{tot}(t'_s)] \cdot [\mathbf{p}_s - \mathbf{A}_{tot}(t'_s)]}{2} + I_p = 0 \end{aligned} \quad (1)$$

where I_p is the ionisation potential of the atom, ω is the harmonic frequency, $\mathbf{A}_{tot}(t)$ is the vector potential associated to $\mathbf{E}_{tot}(t)$, and t_s and t'_s are the stationary values of the recom-

bination and ionisation instants of the electronic wave packet, respectively. The stationary momentum $\mathbf{p}_s$ is given by:

$$\mathbf{p}_s = \frac{1}{t - t'} \int_{t'}^{t} \mathbf{A}_{tot}(t'')dt'' \tag{2}$$

The complex solutions $(\mathbf{p}_s, t_s, t'_s)$ of Eqs. (1-2) identify the most relevant contributions to the XUV spectrum emitted by a single atom.

For each temporal delay τ between the driving and unknown fields, we considered only the solution corresponding to the short path with the highest cut-off frequency[6]. The harmonic spectrum $\mathbf{E}(\omega)$ is then given by:

$$\begin{aligned}\mathbf{E}(\omega) = \frac{i\ 2\pi}{\sqrt{\det(S'')}} \Big[\frac{\pi}{\epsilon + i(t_s - t'_s)/2}\Big]^{3/2} \mathbf{d}^*[\mathbf{p}_s - \mathbf{A}_{tot}(t_s)] \times \\ \times\ \mathbf{E}_{tot}(t'_s) \cdot \mathbf{d}[\mathbf{p}_s - \mathbf{A}_{tot}(t'_s)]\ \exp[-iS(\mathbf{p}_s, t_s, t'_s) + i\omega t_s]\end{aligned} \tag{3}$$

where S is the dipole phase, $\det(S'')$ is the determinant of the matrix of the second time derivative of the phase $(\omega t - S)$ with respect to t and t' evaluated in correspondence of the saddle points solutions $(\mathbf{p}_s, t_s, t'_s)$, ϵ is a regularisation constant, and $\mathbf{d}$ is the gaussian form of the dipole matrix element[5]. The component of the XUV spectrum along the polarisation of the driving field dominates the total signal and we neglect the perpendicular XUV component in the following discussion.

The binary 0-π plate introduced a π-shift between the two halves of the pump beam, thus leading to two focal spots that will be indicated as a and b. The distance between the two spots was measured in $2d \simeq 100\ \mu m$. The XUV spectra generated in the focal spot without (spot a; reference field $E^{ref}_{XUV}(\omega)$) and with the influence of the unknown, perturbing field (spot b; perturbed field $E^{pert}_{XUV}(\omega)$) are given by:

$$\begin{aligned}E^{ref}_{XUV}(\omega) &= E^{ref}(\omega) \exp[i\varphi^{ref}(\omega)] \\ E^{pert}_{XUV}(\omega) &= [E^{ref}(\omega) + \Delta E(\omega)] \exp[i(\varphi^{ref}(\omega) + \Delta\varphi(\omega))]\end{aligned} \tag{4}$$

where $\Delta E(\omega)$ and $\Delta\varphi(\omega)$ indicate the variations in the amplitude and phase introduced by the perturbing field, respectively.

The total XUV electric field $E_{XUV}(x, y, z = 0, \omega)$ in the high-order harmonic generation plane $(z = 0)$ was described as the sum of identical gaussian beams, spaced by $2d$, multiplied

by the spectra given in Eq. 4:

$$\begin{aligned} E_{XUV}(x,y,z=0,\omega) &= E_a(x,y,0,\omega) + E_b(x,y,0,\omega) = \\ &= \exp(-x^2/w_{0x}^2)\exp[-(y-d)^2/w_{0y}^2]E_{XUV}^{ref}(\omega) + \\ &+ \exp(-x^2/w_{0x}^2)\exp[-(y+d)^2/w_{0y}^2]E_{XUV}^{pert}(\omega) \end{aligned} \tag{5}$$

where $w_{0x,y}$ indicate the beam waists in the x and y direction, respectively. In the simulations we considered $w_{0x} = 40\ \mu m$ and $w_{0y} = 20\ \mu m$.

The XUV spectrometer dispersed and focused the harmonic components along the x-direction on its imaging plane (placed at a distance z_0 from the source point), while the two XUV fields freely propagates in the y-direction. In this plane the intensity distribution is characterised by an interference term between the two sources, which is proportional to:

$$E^{ref}(\omega)[E^{ref}(\omega) + \Delta E(\omega)]\exp[i(2kyz_0/R_y) - \Delta\varphi(\omega))] \tag{6}$$

where $k = 2\pi c/\omega$ (c speed of light) and $R_y = z_0[1 + (kw_{0y}^2/(2z_0))^2]$.

The Fourier transform of the signal along the y-direction is characterised by a peak with spatial frequency $2kz_0/R_y$. The amplitude and phase modulations of this peak as a function of the delay τ correspond to $\Delta E(\omega;\tau)$ and $\Delta\varphi(\omega;\tau)$ and were used for the reconstruction of the perturbing field from the simulations and experimental data (see Fig. 1 and Fig. 3 of the manuscript, respectively).

We implemented also a different algorithm based on the analysis of a single interference fringe. In this case, we evaluated the centre of mass of a single fringe for each delay step τ. The results are presented in Fig. 2, which reports the phase retrieved by the Fourier (solid line) and the centre of mass analysis (dashed line) for the measurement shown in Fig. 3 of the manuscript. The two methods present an overall good agreement.

Experimental electric field reconstruction of pulses with time-dependent polarisation and calibration procedure

In the PG scheme, the angles of polarisation of the isolated attosecond pulses ($\gamma_{1,2}$) with respect to the input polarisation direction of the driving field, for the rotation angles $\alpha_{1,2} = \pm 45^\circ$ of the birefringent quartz delay plate, depend on its thickness and on the central wavelength of the pulse. If the plate corresponds to a multiple-order quarter-wave plate of

the fundamental radiation, the polarisation angles are $\gamma_{1,2} = \pm 45°$.

In our experimental conditions, the thickness of the delay plate was determined as the best compromise between the generation of an isolated attosecond pulse with optimal characteristics (in terms of photon flux and absence of satellite pulses), and the requirement to generate XUV pulses with (or close to) perpendicular polarisations when switching between α_1 and α_2.

The field components along the x and y directions ($E_x(t)$, $E_y(t)$) were retrieved from the fields projections $E_1(t)$ and $E_2(t)$, measured along γ_1 and γ_2, using the equations:

$$\begin{bmatrix} E_x \\ E_y \end{bmatrix} = \frac{1}{\cos\gamma_1 \sin\gamma_2 - \sin\gamma_1 \cos\gamma_2} \begin{bmatrix} \sin\gamma_2 & -\sin\gamma_1 \\ -\cos\gamma_2 & \cos\gamma_1 \end{bmatrix} \begin{bmatrix} E_1 \\ E_2 \end{bmatrix} \tag{7}$$

The time-dependent ellipticity $\varepsilon(t)$ of the pulse was evaluated as:

$$\varepsilon(t) = \tan\Big(\frac{1}{2}\arcsin\Big[\frac{2|\tilde{E}_x||\tilde{E}_y|\sin(\varphi_x - \varphi_y)}{|\tilde{E}_x|^2 + |\tilde{E}_y|^2}\Big]\Big) \tag{8}$$

where φ_x and φ_y indicate the phases of the complex components of the electric field $\tilde{E}_x$ and $\tilde{E}_y$, respectively, with $E_{x,y} = \frac{1}{2}(\tilde{E}_{x,y} + \tilde{E}^*_{x,y})$[8].

The XUV spectra generated for α_1 and α_2 presented small differences, which we attributed to the small incidence angle on the focusing and steering mirrors between the PG-unit and the generation cell, and on the finite grazing incidence angle of the attosecond pulses on the XUV optics. As a result, the two polarisation directions γ_1 and γ_2 were not perfectly equivalent and a small amplitude difference and phase shift for the two reconstructed electric field components $E_1(t)$ and $E_2(t)$ was introduced.

In order to minimise these effects, before each measurement, we performed a calibration using a linearly polarised perturbing field (along the x direction, see Fig. 3a of the manuscript). The calibration allowed to determine the correction factor for the ratio of the amplitudes $a = E_1/E_2$ (typically on the order of unit) and for the relative temporal shift t_0 between the two measurements (typically on the order of a few tens of attoseconds). These parameters were then used in the reconstruction of the fields with time-dependent polarisation. The results of a typical calibration are shown in Fig. 3. The small y-component of the field was attributed to a small misalignment of the delay plate.

1. Sansone, G. *et al.* Isolated single-cycle attosecond pulses. *Science* **314**, 443-446 (2006).

2. Ullrich, J. *et al.* Recoil-ion and electron momentum spectroscopy: reaction-microscopes. *Rep. Prog. Phys.* **66**, 1463-1545 (2003).

3. Wittmann, T. *et al.* Single-shot carrier-envelope phase measurement of few-cycle laser pulses. *Nature Phys.* **5**, 357-362 (2009).

4. Feng, C. *et al.* Complete analog control of the carrier-envelope-phase of a high-power laser amplifier. *Opt. Exp.* **21**, 25248-25256 (2013).

5. Lewenstein, M., Balcou, P., Ivanov, M. Y., L'Huillier, A. & Corkum, P. B. Theory of High-Harmonic Generation by Low-Frequency Laser Fields. *Phys. Rev. A* **49**, 2117-2132 (1994).

6. Sansone, G., Vozzi, C., Stagira, S. & Nisoli, M. Nonadiabatic quantum path analysis of high-order harmonic generation: Role of the carrier-envelope phase on short and long paths. *Phys. Rev. A* **70**, 013411 (2004).

7. Sansone, G. Quantum path analysis of isolated attosecond pulse generation by polarisation gating. *Phys. Rev. A* **79**, 053410 (2009).

8. Strelkov, V. *et al.* Generation of attosecond pulses with ellipticity-modulated fundamental. *Appl. Phys. B* **78**, 879-884 (2004).

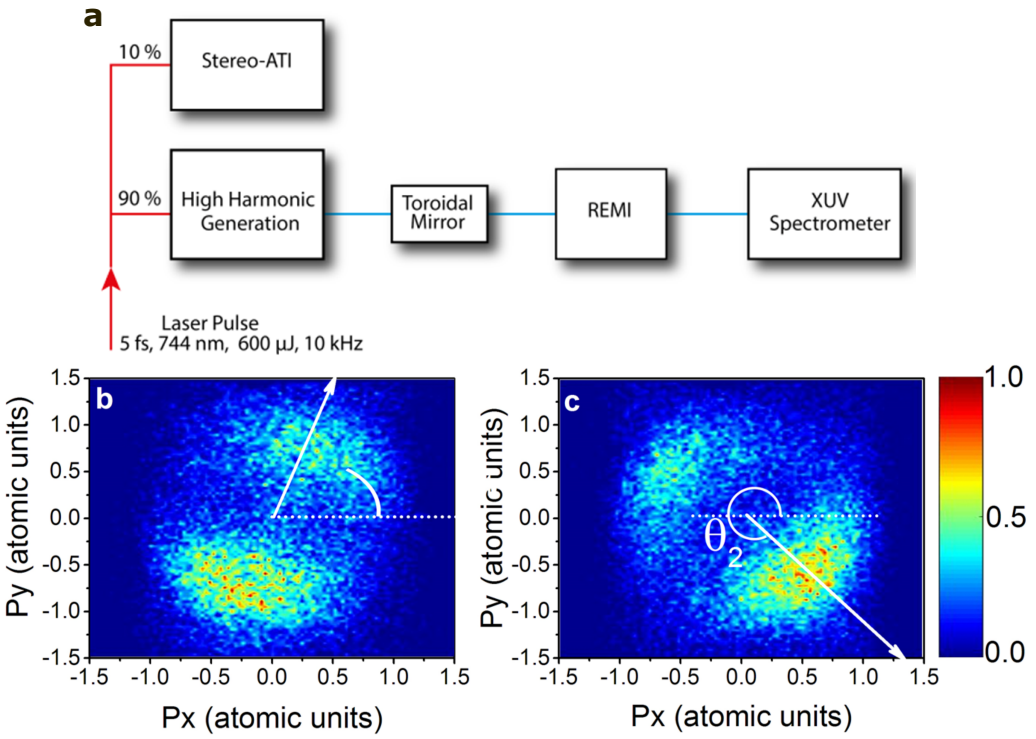

Figure 1. **Experimental beamline and photoelectron angular distributions measured for α_1 and α_2.**

a, Schematic view of the experimental beamline including the REMI, the XUV spectrometer, and the Stereo-ATI. **b**,**c**, Photoelectron angular distributions measured by the REMI for the rotation angles of the delay plate in the PG unit of the driving pulses in the plane perpendicular to the propagation direction $\alpha_1 = 45°$ and $\alpha_2 = -45°$, respectively. The two axis represent the x and y components of the photoelectron momentum. The white solid lines indicate the polarisation of the two attosecond pulses in the interaction region of the REMI.

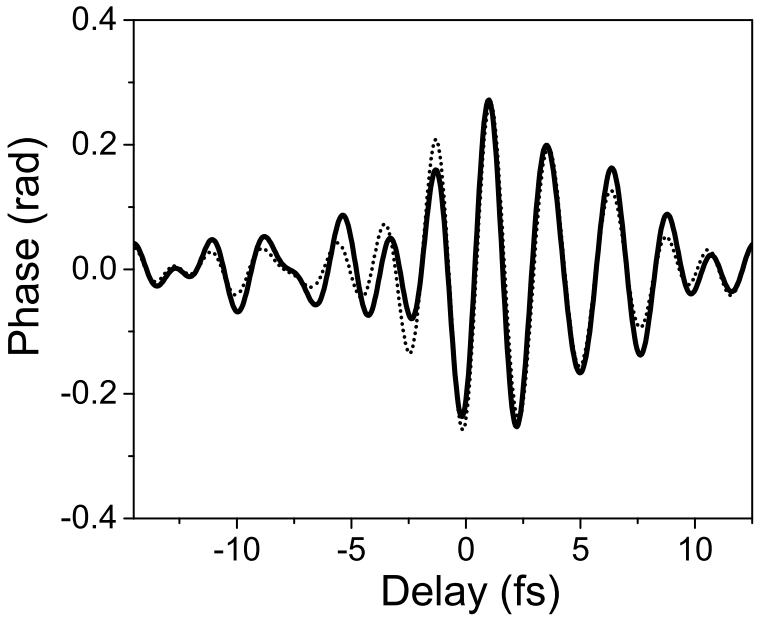

Figure 2. **Data analysis**.

Phase modulation retrieved from the experimental data (Fig. 3 of the manuscript) using the Fourier transform algorithm (solid line) and the single-fringe analysis (short dotted line).

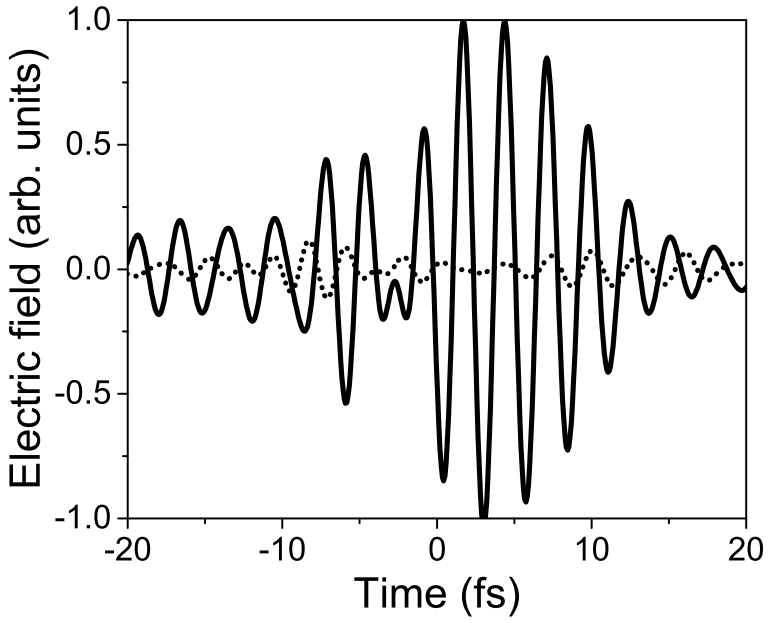

Figure 3. **Calibration for the reconstruction of linearly polarised pulses.**
Electric field components along the x (solid line) and y (short dotted line) directions for nominal linear polarisation along the x direction.